Crystal size effects on giant thermopower in CrSb_{2}

Qianheng Du (□□□), David Guzman, Sangkook Choi, and C. Petrovic

Phys. Rev. B **101**, 035125 — Published 16 January 2020

DOI: 10.1103/PhysRevB.101.035125

Crystal size effects on giant thermopower in $CrSb_2$

Qianheng Du (杜乾衡)[1,2,†], David Guzman[1], Sangkook Choi[1] and C. Petrovic[1,2,‡]
[1]*Condensed Matter Physics and Materials Science Department, Brookhaven National Laboratory, Upton, New York 11973, USA*
[2]*Department of Materials Science and Chemical Engineering, Stony Brook University, Stony Brook, New York 11790, USA*
(Dated: January 6, 2020)

We have examined size effect on thermal, transport and thermodynamic properties of $CrSb_2$ single crystal. We demonstrate highly anisotropic quasi-1D electrical conductivity, quasi-ballistic phonons and giant thermopower of -6 mV/K at 15 K. Thermopower peak is suppressed to -1.6 mV/K by changing crytal dimensions and shows linear dependence on the phonon mean free path. Whereas electronic diffusion thermopower is significant, the bulk of the giant thermopower in $CrSb_2$ stems from the coupling of the very long mean-free-path phonons with the in-gap states.

INTRODUCTION

Materials for cryogenic energy conversion must maximize thermoelectric power factor ($S^2\sigma$) since in the figure of merit $ZT = S^2\sigma \mathrm{T}/\kappa$, where S is thermopower and σ and κ are electrical and thermal conductivity, temperatures are very modest [1]. Furthermore, electronic correlations are rather important [2–7] and consequently FeSi-like narrow gap semiconductors with dominant *3d* character of electronic states near the conduction- and valence-band edges have been attracting considerable attention [8–14]. Due to its colossal thermopower of up to 45 mV/K and rich family of marcasite structures, $FeSb_2$ is an excellent candidate to study the guiding principle of high thermopower materials design [15–24].

An essential property of a thermoelectric material is the phonon transport [25–28]. Phonons carry heat which reduces the thermoelectric efficiency but may also enhance thermopower (S) through the phonon drag effect by contributing to thermoelectric voltage in high purity semiconductors with strong electron-phonon coupling [29]. In $FeSb_2$ crystals colossal thermopower peak was attributed to electron diffusion [17, 19, 20] or to phonon drag effect [30]. $CrSb_2$ crystallizes in the orthorhombic marcasite structure identical to $FeSb_2$, featuring $S \approx -4.5$ mV/K [31]. This is also very large and presently not understood within the diffusion model since commonly observed thermopower values in metals or in semiconductors are typically in (10 - 100) μV/K range [32, 33].

Here we report low-temperature study of thermoelectricity in $CrSb_2$ with controlled size reduction. We observe thermopower peak of -6 mV/K at 15 K, higher than in previous report [31] and nearly balistic phonons with mean free path (MFP) of about 0.6 mm at low temperatures. The peak is compressed to -1.6 mV/K by decreasing crystal dimension. Thermopower value is proportional to the phonon mean free path (MFP) at its peak temperature whereas the size-reduction induced decrease is attributed to the reduction of the phonon MFP due to crystal-boundary scattering.

EXPERIMENTAL DETAILS

Single crystals of $CrSb_2$ were grown as described previously [31]. Crystal structure was confirmed by analyzing powder X-ray diffraction (XRD) pattern taken with Cu $K\alpha$ radiation ($\lambda = 1.5418 \mathring{A}$) of a Rigaku Miniflex X-ray machine. Crystal was oriented using a Laue camera and cut along a-, b- and c-axis for resistivity, thermopower and thermal conductivity measurement. In order to study the size effect, a bar-shaped sample was cut from a big single crystal along the b-axis and then polished into different dimensions step by step to yield six different crystals S1 - S6 for the thermal transport measurement after each polishing step. Heat capacity was measured on a piece of single crystal cut from the same bar-shaped sample. Hall effect is measured using the same crystal with current along the b-axis and field along the c-axis. Thermal transport, heat capacity and electrical transport were measured in separate experiments using Quantum Design PPMS-9. The electronic structure calculations of $CrSb_2$ in the antiferromagnetically ordered state were carried out using density functional theory (DFT) as implemented in the Vienna ab-initio simulation package (VASP)[34, 35]. Projector-augmented-wave (PAW) potentials[36, 37] were used to account for the electron-ion interactions, and the electron exchange-correlation potential was calculated using the local density approximation (LDA) as well as the LDA + U [38] approaches. For the LDA + U calculations, the Coulomb and exchange parameters (U and J) for Cr-d orbitals are taken as U=2.7 eV and J=0.3 eV [38]. The kinetic energy cutoff was set to 500 eV and the Brillouin zone integration was performed on a dense Γ-centered 10×4×9 k-mesh with 132 irreducible k-points using Gaussian smearing with a width of 0.02 eV. The lattice parameters and atomic positions of $CrSb_2$ are kept at their experimental values[39].

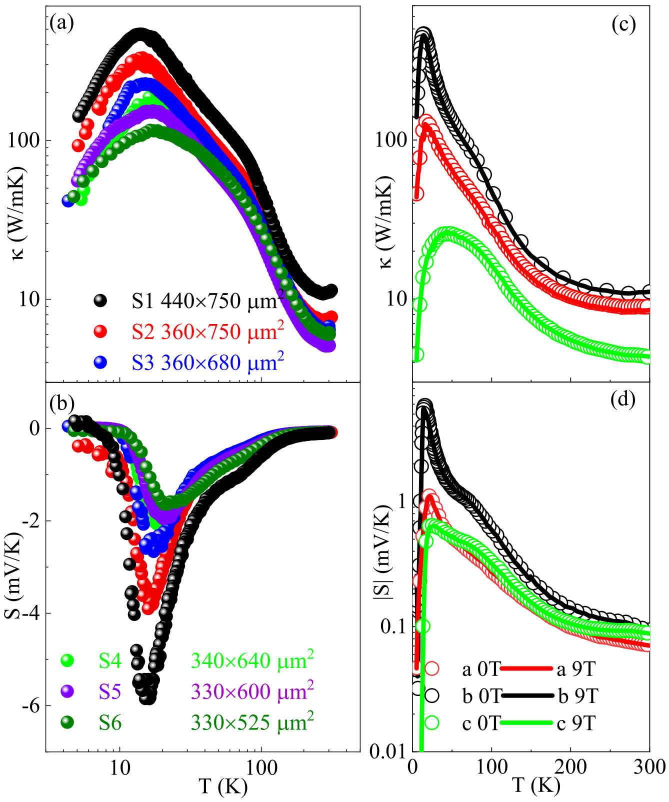

FIG. 1. Size dependence of the thermal transport properties, (a) thermal conductivity κ and (b) thermopower S for thermal gradient along the b-axis. Both S and κ show strong size dependence. (c,d) show κ and S along different crystal axes in zero and in 9 T magnetic field. Note that anisotropy in $S(T)$ and $\kappa(T)$ are similar.

RESULTS

Both thermal conductivity κ and thermopower S reveal a significant sample-size effect [Figure 1(a,b)]. The sample S1 shows the largest thermopower value of $|S| = 6$ mV/K at 15 K. The maximum value decreases to 1.6 mV/K (S6) with decreasing sample cross-section. Similar to the size dependence of S, the maximum κ also decreases from 550 $\mathrm{Wm^{-1}K^{-1}}$ (S1) to 125 $\mathrm{Wm^{-1}K^{-1}}$ (S6). Since the electronic thermal conductivity κ_e calculated from Wiedemann-Franz law is negligible, the size effect on κ must come from the phonon transport. Phonon drag mechanism is likely involved in the low-temperature thermopower enhancement due to similar dependence on the size reduction and similar temperature range of the thermopower and thermal conductivity peaks [Fig. 1(a,b)]. Even though there is a strong anisotropy of thermopower and thermal conductivity when thermal gradient is applied along different crystalline axes, S and κ are independent of magnetic field [Fig. 1(c,d)]. This argues in favor of the decisive role of phonons and against the electronic mechanism of the enhancement.

Figure 2(a) shows anisotropy in resistivity ρ for electric current applied along all three crystallographic axes of the orthorombic unit cell. The temperature dependence of resistivity is similar, albeit with considerable differences in magnitude. The highest conductivity is observed along the crystallographic c-axis. This is the direction of one dimensional (1D) antiferromagnetic chains [40]. The observation of weak inflection point at the Néel temperature $T_N \approx 273$ K for ρ_c and the absence of such anomaly for ρ_a and ρ_b shows that quasi 1D magnetic scattering is dominant only in [001] direction, in agreement with the observed influence of magnetic anisotropy on thermal conductivity [40]. Thermally activated resistivity is observed for electrical transport along all directions [Fig. 2(b)]. The resistivity data can be described by $\rho \propto exp(\Delta/2k_BT)$ with different gaps: $\Delta_1 \approx$ (68.9-96.0) meV in the intrinsic regime $100 < T < 300$ K, $\Delta_2 \approx$ (12.1-20.0) meV for $16 < T < 33$ K in the region of high thermopower and $\Delta_3 \approx$ (0.28-0.38) meV for $T < 10$ K. Then, the temperature dependence of the resistivity is consistent with a slightly doped narrow-gap semiconductor. Figure 2(c) shows the Hall effect measured in the same crystal at 15 K, 40 K and 80 K. The Hall effect shows clear linear behavior and the calculated carrier concentration is $n_e = 2.95(1)\times10^{22}$ $\mathrm{m^{-3}}$ at 15 K near thermopower peak, in agreement with previous report [31]. Carrier mobility from the Drude model [$\rho = 1/ne\mu$] is $8.4(1)\times10^{-3}\mathrm{m^2/Vs}$ at the same temperature. From the Hall data at higher temperatures we evaluate $n_e = 4.00(1)\times10^{23}$ $\mathrm{m^{-3}}$ and $\mu = 2.1(1)\times10^{-2}\mathrm{m^2/Vs}$ at 40 K, $n_e = 1.14(1)\times10^{24}$ $\mathrm{m^{-3}}$ and $\mu = 7.6(1)\times10^{-3}\mathrm{m^2/Vs}$ at 80 K.

Figure 2(d) shows the heat capacity of the $CrSb_2$ crystal. By fitting the low temperature data [Fig. 2(e)] using the Debye model $C_v = \frac{12\pi^4}{5}R(\frac{T}{\theta_D})^3 + \gamma T$, the Debye temperature $\theta_D = 291.1(1)$ and Sommerfeld coefficient $\gamma \approx 0$ are obtained. The sound velocity ν_s is ≈ 2800 ms^{-1} evaluated from θ_D=(h/k$_B$[(3qNρ)/(4πM)]$^{1/3}\nu_s$ where h, k_B are Planck and Boltzmann constants, q is the number of atoms, M is the molar mass, N is Avogadro's number and ρ is the density [41]. Next, we will evaluate the temperature-dependent phonon MFPs which are closely related to phonon transport using Fourier's law ($\kappa = \frac{1}{3}C\nu l_\kappa$) with the Debye model, where C, ν and l_κ are the specific heat, phonon velocity and MFPs of the phonon involved in the thermal conductivity, respectively. Using these values, we calculated the MFPs below 20 K for all crystals S1 - S6; the results are shown in Figure 2(f).

The phonon MFPs are quasi-ballistic, on the order of 100 μm to 0.6 mm at low temperature and comparable to sample size. This suggests that MFPs may be dominated by crystal-boundary scattering where sample surfaces act as diffuse phonon scatterers. When phonons are scattered at the crystal surface, boundary-scattering-dominated mean free path l_b for the rectangular-shape

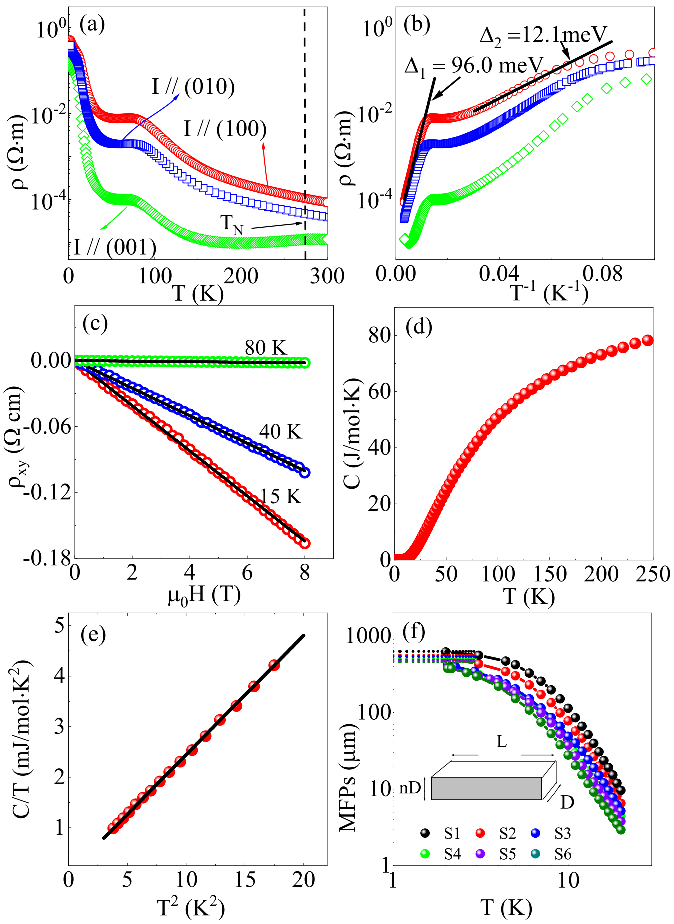

FIG. 2. Temperature dependence of the electrical resistivity for S1 with current along all three principal crystallographic axes (a,b). Note about two orders of magnitude higher conductivity when I // c-axis. Different regions of activated transport are noted in (b). (c) Hall effect measured at several different temperatures. The open symbols show the data and the black lines show the linear fit. (d) Heat capacity of $CrSb_2$ crystal and (e) Debye model fits in the low temperature range. (f) Phonon mean free paths vs. temperature below 20 K. When compared to about 1 nm at 15 K and 7 nm at 40 and 80 K electron mean free path, the phonon MFPs are much longer. Dotted lines represent the crystal surface-dominated mean free path l_b for each sample. Inset shows sample shape.

sample with side dimensions D and nD [Fig. 2(f) inset] is [42, 43]:

$$l_b = (\frac{1}{4}Dn^{1/2})[3n^{1/2}ln\{n^{-1} + (n^{-2}+1)^{1/2}\}$$
$$+ 3n^{-1/2}ln\{n + (n^2+1)^{1/2}\}$$
$$- (n+n^3)^{1/2} + n^{3/2} - (n^{-1}+n^{-3})^{1/2} + n^{-3/2}]$$

This estimate is valid when crystal length L is much

Sample No.	L_s (μm)	A ($10^{-43}s^3$)	B ($10^{-17}sK^{-1}$)	L (μm)	l_b (μm)	D (μm)
S1	620	1.25	0.91	5250	630	440
S2	510	2.25	0.95	5250	560	360
S3	480	3.23	0.73	5250	538	360
S4	450	3.42	0.60	5250	507	340
S5	430	3.61	0.84	5250	485	330
S6	400	4.13	0.90	5250	460	330

TABLE I. Fitting parameters L_s, A and B for the thermal conductivity κ of different samples. The L, l_b and D are listed for comparison.

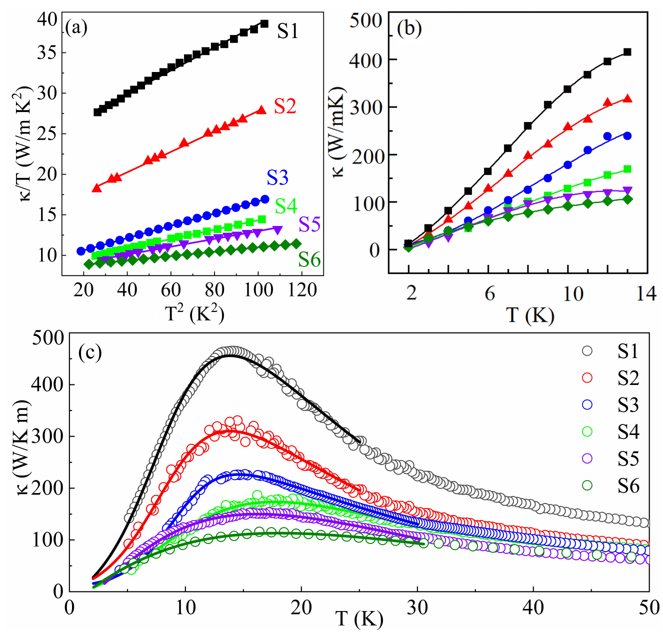

FIG. 3. Temperature dependence of the thermal conductivity in low temperature. (a,b) The fitting of κ/T vs T^2 and κ vs T. The solid lines are fitting results. (a) and (b) share the same legend. (c) Thermal conductivity below 50 K. The solid lines are fitting of Callaway model.

larger than the phonon mean free path, whereas phonon mean free path l_b~D, i.e. L≫l_b~D. This is satisfied in our experiment. By using this equation, the l_b for samples S1, S2, S3, S4, S5 and S6 are estimated to be 630, 560, 538, 507, 485 and 460 μm, respectively. The experimental data at low temperature approach the estimated limits [dotted lines in Figure 2(f)]. According to the Debye theory, if the thermal conductivity is dominated by surface (boundary) scattering, the κ will show T^3 power law. From fitting the κ/T vs T^2 which show good linear relationship and the κ vs T which show direct $\kappa \propto T^3$ power law, the boundary scattering seems to dominate the low temperature thermal conductivity [Fig. 3(a,b)]. In order to confirm the role of boundary scattering in determining the MFPs, the Callaway model was used to fit the thermal conductivity. In Callaway model,

$$K_L = \frac{k_B}{2\pi^2 \nu_s}(\frac{k_B}{\hbar})^3 T^3 \int_0^{\frac{\theta_D}{T}} \frac{\tau x^4 e^x}{(e^x - 1)^2} dx$$

where $x = \frac{\hbar\omega}{k_B T}$ is dimensionless, ω is the phonon frequency, k_B is the Boltzmann constant, $\hbar$ is the Plank constant, θ_D is the Debye temperature, ν_s is the velocity of sound and τ is the overall relaxation time. The overall relaxation time τ can be determined by combining different scattering processes [23]

$$\begin{aligned} \tau^{-1} &= \tau_B^{-1} + \tau_I^{-1} + \tau_U^{-1} \\ &= \frac{\nu_s}{L_s} + A\omega^4 + B\omega^2 T e^{-\frac{\theta_D}{T}} \end{aligned}$$

where τ_B, τ_D, τ_U are the relaxation times for boundary scattering, impurities scattering, and Umklapp processes, respectively. The L_s, A and B are fitting parameters. The L_s represents the boundary scattering length. The fitting results are shown in Fig. 3(c). The fitting parameters are listed in Table 1. The sample dimensions L, D, and MFP l_b are listed for comparison. The results support dominant scattering of phonons by sample surfaces.

The chemical potential corresponding to the density of free carriers at 40K ($n_e = 4 \times 10^{23} m^{-3}$) and 80K ($n_e = 1.14 \times 10^{24} m^{-3}$) was determined by numerical integration of the electronic density of states computed at the DFT-LDA+U level. Figure 4(a) shows the density of states (DOS) and electron density as function of energy between the top of the valence band and 1 eV. The inset in Fig. 4(a) zooms-in into the energy range corresponding to the measured free carrier density. The resulting chemical potential is calculated to be approximately 403 meV for both carrier densities. Electronic band dispersion is shown in Figure 4(b), where the blue dot line indicates the chemical potential (μ) corresponding to the measured free carrier densities. It should be noted that only one band crosses this chemical potential.

The effective mass of carriers is:

$$\left(\frac{1}{m^*}\right)_{ij} = \frac{1}{\hbar^2} \frac{\partial^2 E_n(\vec{k})}{\partial k_i k_j}; i,j = x,y,z$$

where i, j are the components in reciprocal space and $E_n(\vec{k})$ is the n_{th} band energy dispersion relation. The second and cross derivatives in the symmetric tensor of equation 1 are numerically calculated on a five-point stencil with a 0.05 step size [44].

Based on the DFT-LDA+U electronic band structure, the effective mass tensor of the conduction band crossing the chemical potential μ, Figure 4(b), and with minimum around the T high symmetry point is:

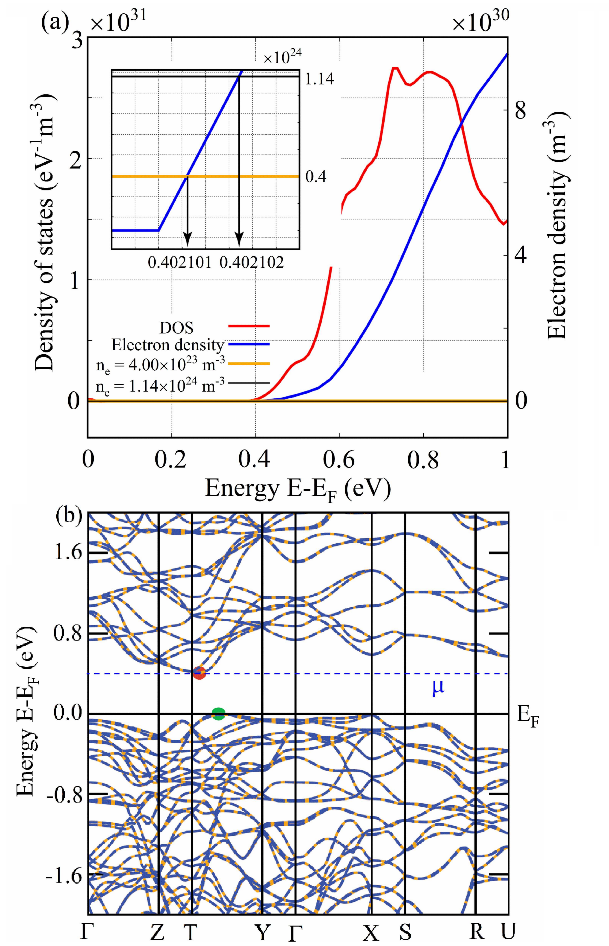

FIG. 4. (a) Density of states (red) and electron density (blue) as function of energy. The inset shows the energy range corresponding to the measured carrier densities. (b) Electronic band dispersion showing the chemical potential corresponding to the measured carrier densities. The Fermi energy has been set to zero. The red and green spots represent the minimum of conduction band and maximum of valence band, respectively.

$$\left(\frac{m^*}{m_e}\right)_{LDA+U} = \begin{pmatrix} 0.470 & 0.00 & 0.00 \\ 0.00 & 1.130 & 0.108 \\ 0.00 & 0.108 & 0.606 \end{pmatrix}$$

We note that the LDA+U computed effective masses show an enhancement of about two times compared to the LDA result, which produces a effective mass tensor of:

$$\left(\frac{m^*}{m_e}\right)_{LDA} = \begin{pmatrix} 0.271 & 0.00 & 0.00 \\ 0.00 & 0.621 & 0.081 \\ 0.00 & 0.081 & 0.334 \end{pmatrix}$$

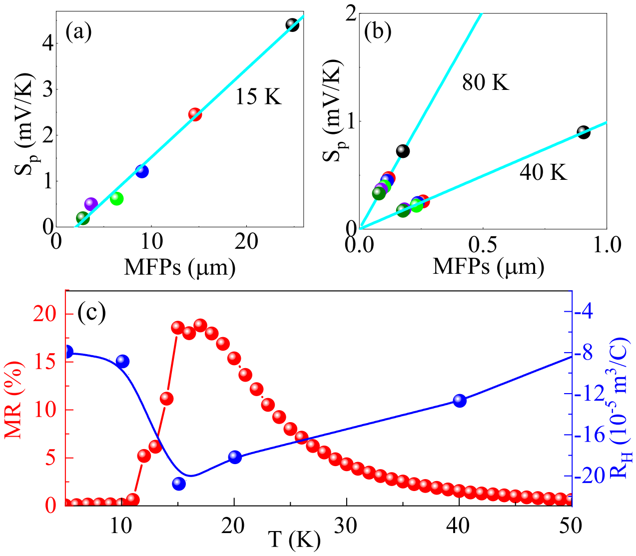

FIG. 5. (a,b) Phonon thermopower values for crystals S1 - S6 as a function of the phonon mean free paths at the corresponding temperatures. The solid line is the linear fitting of the data revealing the linear dependence of S on the phonon MFPs. (c) Magnetoresistance and Hall coefficient R_H vs temperature below 60 K.

DISCUSSION

In general, both electronic diffusion S_d and phonon drag S_p contribute to thermopower. The S_d for a single band degenerate system is $S_d = \frac{8\pi^2 k_B^2}{3eh^2} m^\star T(\frac{\pi}{3n})^{2/3}$ where $m^\star$ is the carrier effective mass and n is the carrier concentration [20, 45, 46]. Using the carrier concentration from Hall effect and $m^\star = 1.13m_e$ (m_e is electron mass) the calculated S_d is $\sim$ 1.19 mV/K at 15 K, a significant value. By subtracting this value from the total S at peak temperature of thermopower of S1-S6, we estimate contribution of S_p. As shown in Figure 5(a,b), there is a linear dependence of phonon-drag thermopower maxima on phonon MFP in all S1 - S6 crystals, implying overwhelming contribution of the phonon drag.

Phonon-drag component of S is proportional to $\beta\nu l\mu^{-1}T^{-1}$, where l is the MFP of the phonons involved in the phonon-drag effect, μ is the carrier mobility, and β is a parameter between 0 and 1 characterizing the relative strength of electron-phonon interaction [47]. If carriers are scattered only by phonons β is 1, but additional scattering processes can significantly reduce its value. Furthermore, the saturation effect, i.e. the correction for high carrier concentration must considered due to relatively high carrier concentration in $CrSb_2$ [47, 48]. The corrected phonon-drag part thermopower becomes $S_p = (\frac{\mu T}{\beta\nu l} + \frac{3ne\beta\nu T}{N_d k_B \mu T})^{-1}$, where N_d is the number of phonon modes that interact with the charge carriers. Using the calculated S_p and values of carrier concentration and mobility obtained in Hall measurement [Fig. 2(c)], the calculated β is about 0.91 around peak temperature of 15 K. Similar calculations show that β is around 1 up to 80 K [Fig. 5(b)]. This strongly suggests that the thermopower in $CrSb_2$ at 80 K and below is dominated by the phonon drag effect on carriers experiencing additional electronic correlations. As the temperature is lowered to 15 K thermal conductivity and thermopower [Fig. 1(a,b)] are reduced in similar manner as the mean free path of phonons is reduced [Fig. 2(f)], confirming the decisive part of phonon drag in giant thermopower of $CrSb_2$.

If the phonon-drag effect is related to in-gap states, there will be a peak in magnetoresistance (MR) and Hall coefficient and one in-gap state gives only one peak [49]. In order to confirm the origin of the phonon-drag effect, we show the MR $= \rho(B) - \rho(0)/\rho(0)$ and Hall coefficient data below 60 K on Fig. 5. Similar to $FeSb_2$, there is a well defined peak in MR and R_H, implying phonon-drag interaction coupling to the in-gap impurity states.

In summary, we have presented the first direct evidence that $CrSb_2$ is a highly anisotropic, quasi-1D semiconductor. The electronic diffusion component of the thermopower S_d is very large but the bulk of the giant thermopower values in $CrSb_2$ stems from the phonon-drag effect of the long MFPs phonons on the in-gap state. Whereas large S_d could arise from the local correlations-enhanced energy gap [38], further studies of materials-related parameters that lead to simultaneous electron- and phonon-related enhancement of thermopower are of interest.

Work at Brookhaven National Laboratory was supported by US DOE, Office of Science, Office of Basic Energy Sciences under contract DE-SC0012704 (Q. D and C. P.). Electronic calculations were supported by the Center for Computational Materials Spectroscopy and Design (D. G and S. C). This research used resources of the National Energy Research Scientific Computing Center (NERSC), a U.S. Department of Energy Office of Science User Facility operated under Contract No. DE-AC02-05CH11231.

‡petrovic@bnl.gov †qdu@bnl.gov

[1] G. J. Snyder, E. S. Toberer, Nat. Mater. **7**, 105 (2008).
[2] Gunnar Palsson and Gabriel Kotliar, Phys. Rev. Lett. **80**, 4775 (1998).
[3] W. Koshibae and S. Maekawa, Phys. Rev. Lett. **87**, 236603 (2001).
[4] Machhindra Koirala, Hui Wang, Mani Pokharel, Yucheng Lan, Chuanfei Guo, Cyril Opeil, and Zhifeng Ren, NANO Lett. **14**, 5016 (2014).
[5] Yiqun Zhang, M. S. Dresselhaus, Yi Shi, Zhifeng Ren and Gang Chen, NANO Lett. **11**, 1166 (2011).
[6] Yang Wang, Yu Sui, Peng Ren, Lan Wang, Xianjie Wang, Wenhui Su and Hongjin Fan, Chem. Mater. **22**, 1155 (2010).

[7] Y. Ando, N. Miyamoto, K. Segawa, T. Kawata and I. Terasaki, Phys. Rev. B **60**, 10580 (1999).
[8] V. Jaccarino, G. K. Wertheim, J. H. Wernick, L. R. Walker, and S. Arajs, Phys. Rev. **160**, 476 (1967).
[9] D. Mandrus, J. L. Sarrao, A. Migliori, J. D. Thompson, and Z. Fisk, Phys. Rev. B **51**, 4763 (1995).
[10] B. C. Sales, E. C. Jones, B. C. Chakoumakos, J. A. Fernandez-Baca, H. E. Harmon, J. W. Sharp, and E. H. Volckmann, Phys. Rev. B **50**, 8207 (1994).
[11] R. Wolfe, J. H. Wernick, and S. E. Haszko, Phys. Lett. **19**, 449 (1965).
[12] L. DeGiorgi, M. B. Hunt, H. R. Ott, M. Dressel, B. J. Feenstra, G. Grüner, Z. Fisk, and P. Canfield, Euro. Phys. Lett. **28**, 341 (1994).
[13] J. M. Tomczak, K. Haule, and G. Kotliar, Proc. Natl. Acad. Sci. (USA) **109**, 3243 (2012).
[14] V. V. Glushkov, I. I. Lobanova, V. Yu. Ivanov, V. V. Voronov, V. A. Dyadkin, N. M. Chubova, S. V. Grigoriev and S. V. Demishev, Phys. Rev. Lett. **115**, 256601 (2015).
[15] C. Petrovic, J. W. Kim, S. L. Bud′ko, A. I. Goldman, P. C. Canfield, W. Choe and G. J. Miller, Phys. Rev. B **67**, 155205 (2003).
[16] C. Petrovic, Y. Lee, T. Vogt, N. Dj. Lazarov, S. L. Bud′ko, and P. C. Canfield, Phys. Rev. B **72**, 045103 (2005).
[17] A. Bentien, S. Johnsen, G. K. H. Madsen, B. B. Iversen, and F. Steglich, Euro. Phys. Lett. **80**, 17008 (2007).
[18] H. Takahashi, R. Okazaki, Y. Yasui, and I. Terasaki, Phys. Rev. B **84**, 205215 (2011).
[19] P. Sun, M. Søndergaard, B. B. Iversen, and F. Steglich, Ann. Phys. (NY) **523**, 612 (2011).
[20] P. Sun, N. Oeschler, S. Johnsen, B. B. Iversen and F. Steglich, Phys. Rev. B **79**, 153308 (2009).
[21] H. Holseth, A. Kjekshus, and A. F. Andersen, Acta Chem. Scand. **24**, 3309 (1970).
[22] H. Takahashi, Y. Yasui, I. Terasaki, and M. Sato, J. Phys. Soc. Jpn. **80**, 054708 (2011).
[23] K. Wang, R. Hu, J. Warren, and C. Petrovic, J. Appl. Phys, **112**, 013703 (2012).
[24] Chang-Jong Kang and Gabriel Kotliar, Phys. Rev. Mater. **2**, 034604 (2018).
[25] O. Delaire, K. Marty, M. B. Stone, P. R. C. Kent, M. S. Lucas, D. L. Abernathy, D. mandrus, and B. C. Sales, Proc. Natl. Acad. Sci. (USA) **108**, 4725 (2011).
[26] B. C. Sales, O. Delaire, M. A. McGuire, and A. F. May, Phys. Rev. B **83**, 125209 (2011).
[27] E. S. Toberer, L. L. Baranowski, and C. Dames, Annu. Rev. Mater. Res. **42**, 179 (2012).
[28] A. J. Minnich, J. phys. Condens. Matter **27**, 053202 (2015).
[29] T. H. Geballe, and G. W. Hull, Phys. Rev. **94**, 1134 (1954).
[30] H. Takahashi, R. Okazaki, S. Ishiwata, H. Taniguchi, A. Okutani, M. Hagiwara and I. Terasaki, Nat. Comms. **7**, 12732 (2016).
[31] B. C. Sales, A. F. May, M. A. McGuire, M. B. Stone, D. J. Singh and D. Mandrus, Phys. Rev. B **86**, 235136 (2012).
[32] M. Cutler and N. F. Mott, Phys. Rev. **181**, 1336 (1969).
[33] H. Fritzche, Solid State Comm. **9**, 1813 (1971).
[34] G. Kresse, and J. Furthmüller, Comput. Mater. Sci. **6**, 15 (1996).
[35] G. Kresse, and J. Furthmüller, Phys. Rev. B **54**, 11169 (1996).
[36] G. Kresse, and D. Joubert, Phys. Rev. B **59**, 1758 (1999).
[37] P. E. Blöchl, Phys. Rev. B **50**, 17953 (1994).
[38] G. Kuhn, S. Mankovsky, H. Ebert, M. Regus and W. Bensch, Phys. Rev.B **87**, 085113 (2013).
[39] H. Holseth, and A. Kjekshus, J. Less-common Met. **16**, 472 (1968).
[40] M. B. Stone, M. D. Lumsden, S. E. Nagler, D. J. Singh, J. He, B. C. Sales and D. Mandrus, Phys. Rev. Lett. **108**, 167202 (2012).
[41] O. Andersen, J. Phys. Chem. Solids **24**, 909 (1963).
[42] A. K. McCurdy, H. J. Maris, and C. Elbaum, Phys. Rev. B **2**, 4077 (1970).
[43] C. Hua and A. J. Minnich, Phys. Rev. B **89**, 094302 (2014).
[44] Alexandr Fonari and Christopher Sutton, https://github.com/afonari/emc (2012).
[45] G. S. Nolas, J. Sharp and H. J. Goldsmid, *Thermoelectrics: Basic Principles and New Materials Developments* (Springer, Berlin, 2001).
[46] K. Behnia, D. Jaccard and J. Flouquet, J. Phys. Condens. Matter **16**, 5187 (2004).
[47] C. Herring, Phys. Rev. **96**, 1163 (1954).
[48] H. J. Goldsmid, *Introduction to thermoelectricity*. Springer Series in Materials Science **121**, (2016).
[49] M. Battiato, J. M. Tomczak, Z. Zhong and K. Held, Phys. Rev. Lett. **114**, 236603 (2015).